Wireless Sensing of Complex Dielectric Permittivity of Liquids Based on the RFID

Humberto Lobato-Morales, *Member, IEEE*, Alonso Corona-Chávez, *Senior Member, IEEE*, José Luis Olvera-Cervantes, Ricardo Arturo Chávez-Pérez, and José Luis Medina-Monroy

***Abstract*—A wireless sensing system for the evaluation of the complex dielectric permittivity of solvent liquids is presented. Two sensing tags are proposed for testing of the samples. The first tag is based on a cavity resonator and the second makes use of the epsilon-near-zero effect. Both circuits are designed over the planar substrate-integrated-waveguide (SIW) technology, and operate at 4 GHz. A quartz capillary tube is used for the liquid measurements where only a small amount of sample volume is required. With the addition of planar antennas at the input and output of the sensors, the complete system is implemented for wireless sensing of the materials following the RF identification scheme. The cavity perturbation technique for SIW structures is applied for the dielectric liquid characterization. The proposed sensing tags and system have high potentials for low-cost wireless measurements and real-time monitoring applications.**

***Index Terms*—Dielectric measurements, microwave sensors, RF identification (RFID) tags.**

I. Introduction

THE USE of microwaves for the characterization of materials have been evolved rapidly over the last years [1], [2]. Several applications, including medical, pharmaceutical, industrial, food, and hydrological, among others, are interested in using microwaves for the measurement of the properties of materials due to the use of low-profile sensors, low power-consumption devices, accuracy in the analysis methods, and real-time testing [1]–[7]. Most of the microwave sensors have been designed for the measurement of complex dielectric permittivity of materials as it offers information of the sample-under-test (SUT) properties, such as moisture contents, microwave absorption, density, temperature, among others [1]–[6]. The most used method for dielectric characterization of materials is based on resonant techniques, due to its high accuracy and high sensitivity [5], [6].

In [3], Sarabandi and Li use a microstrip ring resonator operating at 1.25 GHz to analyze the complex dielectric permittivity of different sand samples for the evaluation of moisture contents in each. A cylindrical cavity resonator operating at 2.45 GHz is used and reported in [4] to measure the dependence between temperature and dielectric permittivity of water and ethyl alcohol samples. In [5], Saeed *et al.* report the analysis of dielectric properties of several liquid solvents by using a substrate-integrated-waveguide (SIW) cavity resonator, showing the advantages of the new sensor in terms of lower dimensions and higher accuracy when compared with conventional cavities and planar resonators. The cavity perturbation technique (CPT) for the characterization of dielectric measurements using SIW cavity resonators is presented by Lobato-Morales *et al.* in [6]. A new type of dielectric-permittivity sensor exploiting the epsilon-near-zero (ENZ) effect is proposed by Alu and Engheta in [7]; and the experimental demonstration using an SIW ENZ sensor is reported in [8], achieving even higher sensitivity and smaller dimensions compared with the aforementioned circuits.

As observed, the trend in smaller and more accurate microwave sensors is evolving fast; thus, there have been recent efforts in realizing wireless and portable dielectric-sensing circuits, many of them based on the RF identification (RFID) scheme. Basically, an RFID system provides wireless data capturing where an interrogator circuit is used to scan and identify tagged objects based on the information from the RFID tag. In [9], Preradovic *et al.* present an RFID system based on a chipless planar tag and spectral analysis in which data bits are represented by the coupling (or not) of microstrip resonators operating at different frequencies. The capability of including sensors over a planar RFID tag is demonstrated in [10], where capacitive and resistive elements are added to a single resonator and manipulated, producing variations in resonant frequency and quality factors in the spectral analysis around 2.7 GHz. In [11], Amin and Karmakar propose a coplanar humidity sensor operating at 1 GHz for integration into an RFID tag. In [12], an RFID tag for water-level detection based on microstrip resonators is proposed, performing a spectral analysis from 2.5 to 4 GHz. A method based on time-domain analysis is presented by Girbau *et al.* in [13], where a temperature sensor is integrated into an RFID tag illuminated by wideband frequency pulses. The aforementioned RFID tags are developed over the planar technology without the use of batteries [9]–[13], decreasing costs and complexity of fabrication and maintenance of the circuits.

This paper is an extension of the work in [14], where two types of SIW sensors are proposed for wireless dielectric permittivity measurements of liquids. In this work, the sensors are incorporated into passive tags for wireless measurements; the

Manuscript received November 08, 2013; revised April 30, 2014; accepted June 21, 2014. Date of publication July 08, 2014; date of current version September 02, 2014.

H. Lobato-Morales, R. A. Chávez-Pérez, and J. L. Medina-Monroy are with the Electronics and Telecommunications Department, Centro de Investigación Científica y de Educación (CICESE), Ensenada, Baja California 22860, Mexico (e-mail: hlobato@cicese.mx).

A. Corona-Chávez and J. L. Olvera-Cervantes are with the Electronics Department, Instituto Nacional de Astrofísica, Óptica y Electrónica (INAOE), Puebla 72840, Mexico.

Color versions of one or more of the figures in this paper are available online at http://ieeexplore.ieee.org.

Digital Object Identifier 10.1109/TMTT.2014.2333711

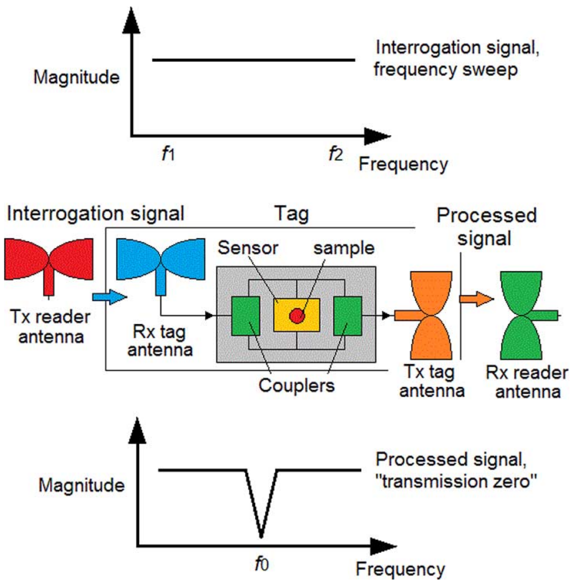

Fig. 1. Basic concept of the proposed wireless RFID sensing system.

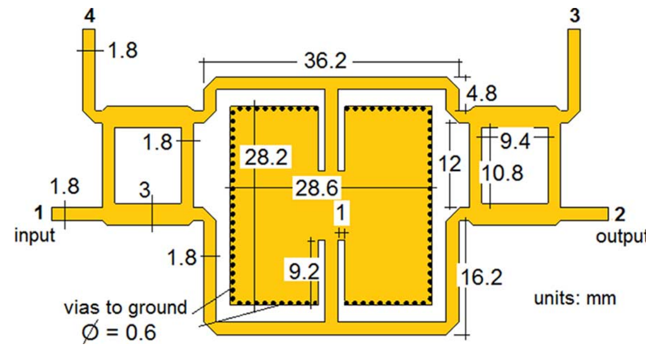

Fig. 2. Geometry and dimensions of *Sensor-A*.

information generated by the tag corresponds to the permittivity characteristics of the liquid under test (LUT). Description of the complete system is presented and the liquid characterization is performed. A low amount of the LUT is required for the measurements and the tag does not make use of any battery, making it an excellent option for wireless and passive real-time sensing or monitoring applications.

This paper is organized as follows. Section II presents the principle of operation of the wireless-sensing system. Section III describes the design and coupling of the sensors. A description of the system is presented in Section IV. The experimental results and liquid characterization are drawn in Section V. Discussions of the results are commented upon in Section VI.

II. Wireless Sensing Principle of Operation

The basic setup of the proposed RFID sensing system is shown in Fig. 1. The principle of operation is as follows: the tag is interrogated by the reader by sending a frequency sweep signal; the receiving (Rx) tag antenna gets the signal and propagates it towards the sensing circuit, which introduces a "transmission zero" with a specific resonant frequency and quality factor Q depending on the tested sample; the processed signal is directed to the transmitting (Tx) tag antenna and sent back to the reader. For minimization of interference between the interrogation and the processed signals, a cross polarization is driven between the pair of antennas carrying the sweep signal (Tx reader and Rx tag antennas) and the pair of antennas communicating the processed signal (Tx tag and Rx reader antennas), as shown in Fig. 1. On the tag, the sensor element is symmetrically fed with the use of hybrid couplers to produce an optimal de-coupling of the signal generating a "transmission zero," which is easily read in such RFID systems [9], [10], and can be further analyzed using the CPT.

III. Design of the SIW Sensors

The proposed sensors are based on the SIW technology using the Rogers RO4003C laminate with dielectric constant $\varepsilon_r = 3.55$ and height $h = 0.813$ mm. The first sensor (*Sensor-A*) is based on an SIW cavity resonator operating in its TE_{101} fundamental mode, and the second sensor (*Sensor-B*) uses an SIW ENZ tunnel structure; both of them operate at 4 GHz. They are symmetrically fed to produce a de-coupling of the signal in order to generate a "transmission zero," which is further analyzed using the CPT for SIW.

A. Sensor-A (SIW Cavity Resonator Sensor)

For *Sensor-A*, dimensions of a TE_{101} SIW cavity resonator operating at 4 GHz are well approximated [5], [15] using

$$f_{101} = \frac{c}{2\sqrt{\varepsilon_r}}\sqrt{\left(\frac{1}{a}\right)^2 + \left(\frac{1}{d}\right)^2} \tag{1}$$

where f_{101} is the resonant frequency, c is the speed of light in a vacuum, and a and d are the width and length of the SIW cavity, respectively. According to (1), the initial cavity dimensions are $a = d = 28$ mm. The cavity is closed by metallic posts (vias to ground) of 0.6-mm diameter separated 0.4 mm between each other [14].

Microstrip hybrid couplers [15] are designed and used to symmetrically feed the cavity. The reasons of using this coupling scheme are: first, to de-couple the signal from the energy flowing from the input to the output in order to obtain the "transmission zero," and second, to strengthen the energy coupled into the cavity as high losses are introduced to the signal along its complete way from the Tx reader antenna through the sensor tag and ending in the Rx reader antenna.

After an optimization process is carried out in simulations [16], Fig. 2 shows the geometry and final dimensions of *Sensor-A*.

In simulations of the lossy structure (dielectric, conductor, and radiation losses) [16], different energy coupling levels are calculated by symmetrically varying the length of the coupling slots l_s. Fig. 3 shows the frequency response of *Sensor-A* for three values of l_s: 2, 6, and 10 mm; and its coupling scheme is shown in the inset of the figure.

From Fig. 3, it is shown that larger slots produce higher couplings. A tight signal coupling is desired, as the energy along all the system will suffer high losses. For the coupling of *Sensor-A*, the length of the slots $l_s = 9.2$ mm is chosen. Although the value $l_s = 10$ mm produces the highest coupling, it is avoided because of the proximity of the slots with the sample position, located at the middle of the cavity, as will be mentioned later.

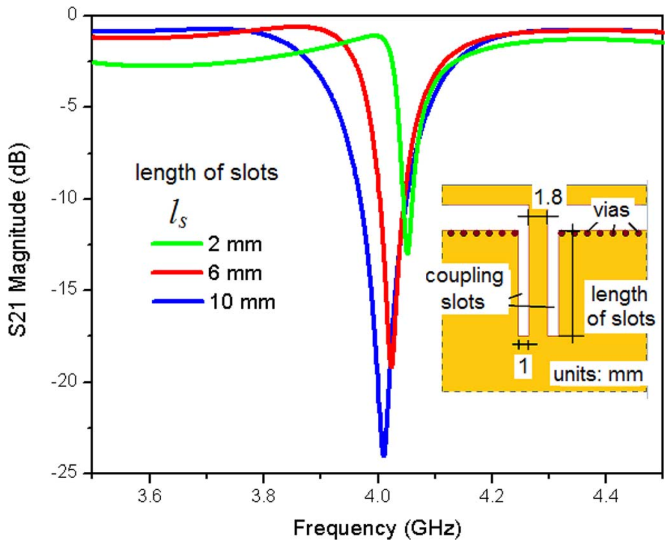

Fig. 3. Simulated frequency response of *Sensor-A* for different coupling levels.

B. Sensor-B (SIW Tunnel Sensor)

The ENZ tunneling phenomenon, described in [7] and [8], is used here for the design of *Sensor-B*. Such an effect can be obtained by coupling a narrow-height waveguide in its TE_{10} propagation mode. Although the coupling is originally made using different-height waveguides to produce squeezing of the energy along the tunnel [7], it is demonstrated that, over the planar SIW technology, the effect can be obtained using transmission lines as coupling elements [17], [18].

The tunneling frequency f_t of an SIW ENZ structure is calculated from the cutoff frequency of a TE_{10} propagation mode SIW waveguide f_{c10} [7] by

$$f_t = f_{c10} = \frac{c}{2b\sqrt{\varepsilon_r}} \tag{2}$$

where b corresponds to the width of the SIW tunnel. The length of the structure is independent on the width and operating frequency. At f_t, a very high and constant electric field is generated inside the SIW waveguide along its length producing the ENZ effect. Initial width of the tunnel operating at 4 GHz results $b = 20$ mm; a tunnel length $l_t = 8.6$ mm is proposed according to dimensions of the complete circuit. The lateral walls of the tunnel are formed by metallic posts (vias to ground) of 0.6-mm diameter spaced 0.4 mm between them.

The ENZ structure is optimized in simulations [16] and connected to hybrid couplers for symmetrically feeding, the same way as for *Sensor-A*. The geometry and final dimensions of *Sensor-B* are shown in Fig. 4; its coupling scheme can be seen in the inset of Fig. 5. As stated in [17] and [18], the coupling level of an SIW ENZ tunnel can be modified by varying the width of the feeding transmission lines. Fig. 5 shows the simulated frequency response of *Sensor-B* with lossy materials (dielectric, conductor, and radiation losses) for three different widths of the feeding lines w_l: 0.2, 1, and 1.8 mm.

It can be appreciated from Fig. 5 that wider feeding lines generate stronger couplings. Width of the lines $w_l = 1.8$ mm is chosen for feeding the tunnel, which corresponds to 50-Ω impedance lines.

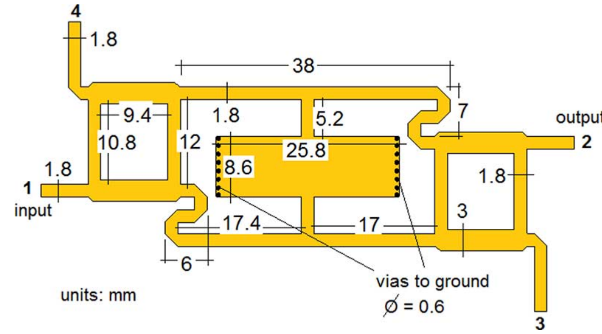

Fig. 4. Geometry and dimensions of *Sensor-B*.

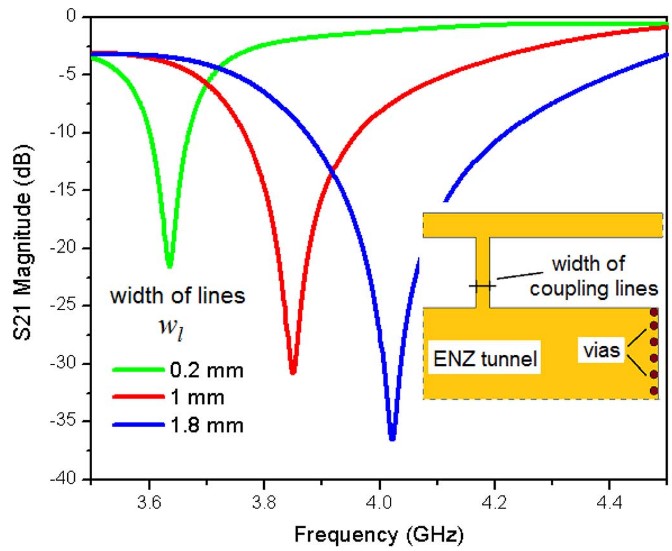

Fig. 5. Simulated frequency response of *Sensor-B* for different coupling levels.

C. Coupling of the Sensors

As the energy in the proposed system is transmitted from the reader to the air, passes along the passive tag, and is returned to the air to be captured back by the reader, the processed data will suffer of high losses; thus, tight couplings of the sensors are desired for this application in order to maintain clarity in the processed signal.

The proposed double-symmetrical coupling scheme for the sensors allows a stronger feeding to the structures compared to single couplings. For that reason, two microstrip hybrids operating at 4 GHz are connected at the input and output of the circuits and optimized to in-phase feed the SIW sensors.

Simulations [16] of the structures with a single-coupling scheme are carried out for comparison purposes. Lossy materials (conductor, dielectric, and radiation losses) are used for the simulations in order to obtain a more realistic scenario. Fig. 6(a) and (b) shows the different frequency responses of the sensors for single and double feeding, and different coupling levels; scheme of the single feeding for the two sensors are shown in the inset.

It is appreciated, from Fig. 6, that stronger couplings are generated by the double-feeding scheme. For the cavity sensor, a maximum coupling of 18.78 dB is achieved with single feeding, while 24.06 dB are obtained with double feeding. For the tunnel sensor, maximum couplings of 31.69 and 36.52 dB are generated with single and double feedings, respectively.

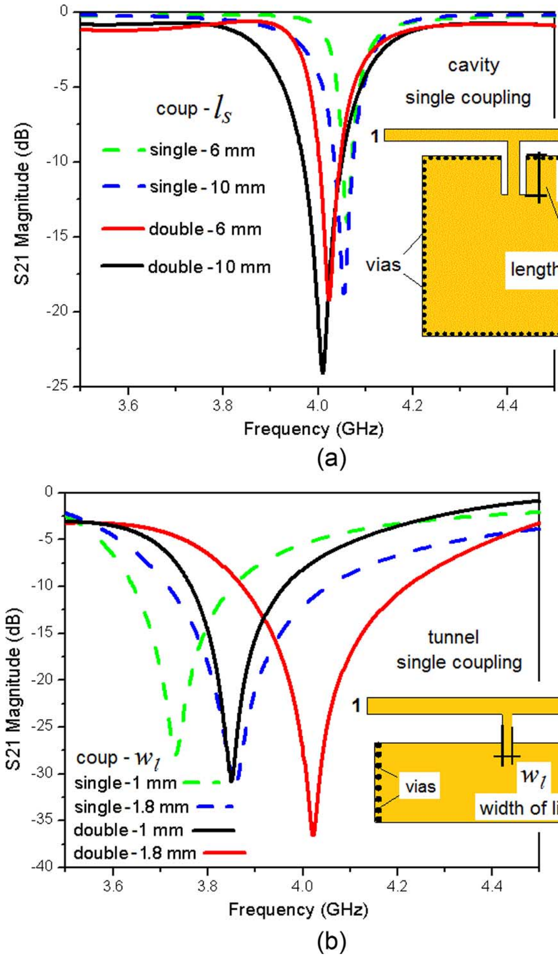

Fig. 6. Frequency responses with single and double feeding for: (a) *Sensor-A* and (b) *Sensor-B*.

The addition of the hybrids occupies an area of 440 mm^2 in each of the sensors; however, enhanced couplings are achieved increasing the accuracy of the measurements in the system [1], [3], [5]–[8]. Ports 3 and 4 of the sensors are terminated with 50-Ω loads.

D. Sample Position

Although both sensors operate under different mechanisms (resonant cavity and tunneling structure), due to their configuration, the maximum electric field $\bar{\boldsymbol{E}}$ occurs at the center of the SIW cavity and tunnel. A quartz capillary tube with outer and inner diameters of 2.5 and 1.5 mm, respectively, is placed perpendicularly to the plane of each sensor through its center; thus, the LUT is interacting with the maximum $\bar{\boldsymbol{E}}$-field producing variations in the frequency responses. With an LUT volume of 1.44 mm^3 it is possible for the sensors to generate the necessary frequency variations. Fig. 7 shows the simulated [19] response of both the structures, using lossless materials, and their electric $\bar{\boldsymbol{E}}$-field distribution.

IV. Implementation of the Wireless Sensing System

Once the sensors are designed, the complete system is implemented with the addition of two antennas to complete the tag (Rx and Tx tag antennas), and other two (Tx and Rx reader antennas) for transmitting the interrogation signal and receiving

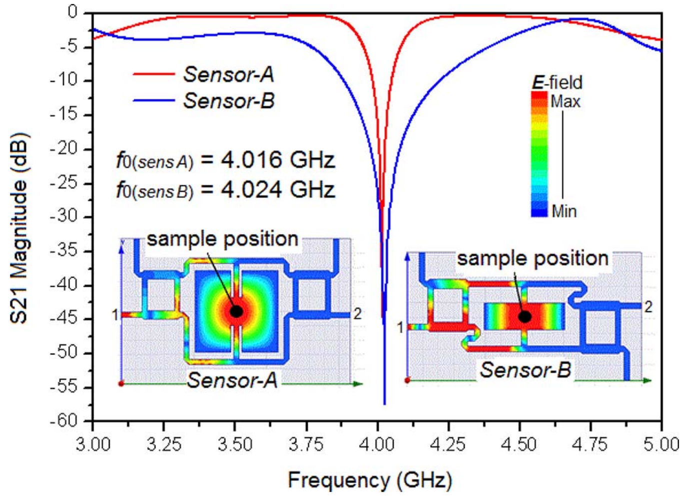

Fig. 7. *Sensor-A* and *Sensor-B* simulated frequency response and $\bar{\boldsymbol{E}}$-field distribution at f_0.

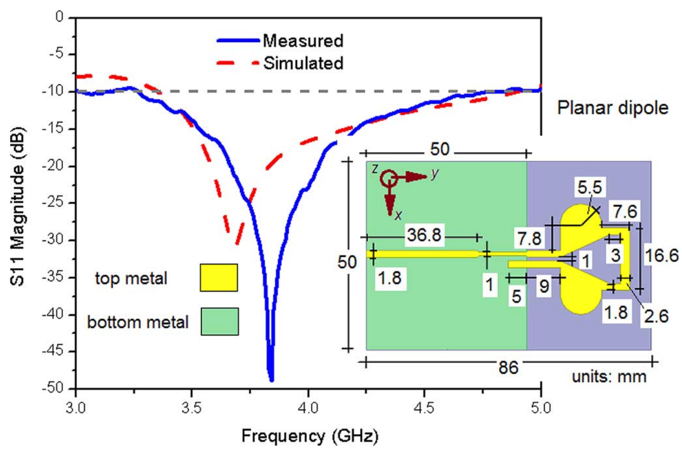

Fig. 8. Frequency response and geometry of the planar dipole antenna.

the processed signal, as shown in Fig. 1. Operation and testing of the designed sensors directly connected to a vector network analyzer (VNA) are reported in [14] for six different liquid samples.

A. Planar Reader Antennas

In the proposed wireless sensing system, the reader is composed by an Agilent N5245A-PNA series VNA connected to planar antennas (Tx reader and Rx reader antennas in Fig. 1) in cross polarization for analysis of the processed signal. Two equal planar closed dipoles are designed based on [20] and optimized in simulations [19] to obtain maximum radiation at 4 GHz. The Rogers RO4003C substrate with $h = 0.813$ is used. The designed dipoles present an experimental bandwidth of $\mathrm{BW}_{di} = 38.5\%$ and its correspondent simulated and measured responses are plotted in Fig. 8, along with dimensions and geometry; their normalized-radiation patterns at 4 GHz in direct polarization are plotted in Fig. 9. From simulations [19] of two dipoles separated 3 cm along their z-axis, an isolation of more than 25 dB is obtained between direct polarization and cross-polarization.

From Fig. 9, it is noticed that maximum radiation with the dipoles is achieved in the $+y$- and $\pm z$-axis directions. The reason why it does not present pure omnidirectional radiation

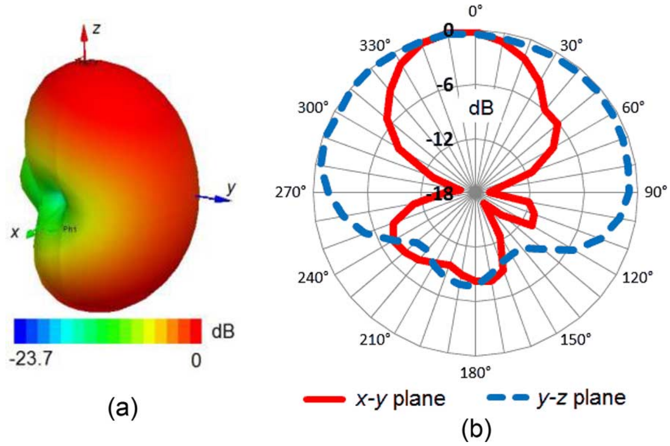

Fig. 9. Normalized radiation pattern of the dipole antennas. (a) Simulated. (b) Measured.

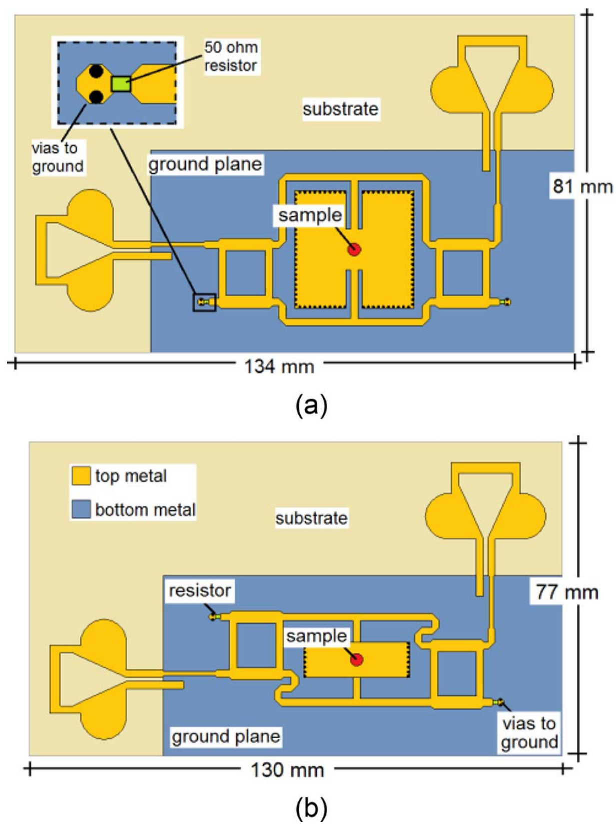

Fig. 10. Geometries of: (a) *Tag-A* and (b) *Tag-B*.

(as expected in dipoles) is thought to be due to their planar feeding lines and ground plane extended in the $-y$-direction.

B. Sensing Tags

For the design of the tags, the planar dipole antennas are connected to the input and output ports of each of the sensors, as shown in Fig. 10; ports 3 and 4 (Figs. 2 and 4) are loaded with 50-Ω on-chip resistors. *Tag-A* and *Tag-B* are implemented with *Sensor-A* and *Sensor-B*, respectively. Overall dimensions of *Tag-A* are 134 mm $\times$ 81 mm, and 130 mm $\times$ 77 mm of *Tag-B*. The Rogers RO4003C substrate with $h = 0.813$ mm is used.

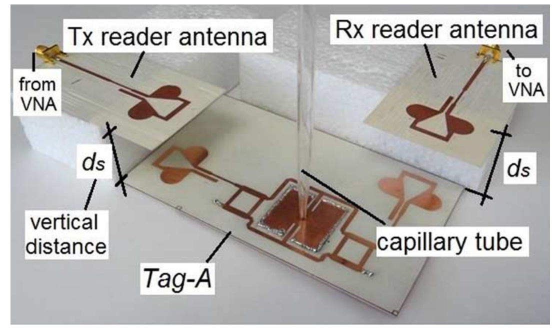

Fig. 11. Photograph of the implemented system with *Tag-A*.

C. Implementation of the System

Fig. 11 shows a photograph of the implemented setup system with the reader antennas and *Tag-A*. The quartz capillary tube is placed vertically through the sensing cavity/tunnel. The reader and tag antennas are vertically aligned along their maximum radiation over the $\pm z$-axes and separated a distance d_s, as shown in Fig. 11.

For measurements with the samples, the VNA is connected to the dipole antennas, which transmit and receive the interrogation and processed signals, respectively; a power output of 0 dBm is generated from the VNA for the interrogation sweep.

V. Measurement and Characterization of the Samples

The LUTs used in the experiment are: 1) acetone; 2) acetonitrile; 3) carbon tetrachloride CCl_4; 4) chlorobenzene; 5) ethanol; 6) isobutanol; 7) isopropyl alcohol; 8) methanol; and 9) xylene. The samples are tested three times inside a temperature-controlled room at 22 °C using both tags, and the measured resonant/tunneling frequencies f_s and quality Q_s factors averaged for the studies. Fig. 12 shows the frequency response of the system using both tags for ethanol, methanol, the empty quartz tube, and without sample, showing the shift in f_s and Q_s at 1-cm separation between the reader and tag antennas d_s (Fig. 11).

As seen in Fig. 12, the "transmission zero" produced by the sensors is clearly defined for the analysis. A wideband frequency response from 3.6 to 4.4 GHz is plotted in Fig. 13 for three different tag distances d_s and with no sample; photographs of the fabricated tags are also shown.

For d_s larger than 1 cm (Fig. 13), the generation of resonances and other peaks outside the region of operation of the system and the shift in the operating frequency are thought to be due to standing waves and interference in the signal along its entire path. Since the operating frequency presents variations for the different tag separations d_s, position of the reader and the tag antennas must remain constant when analyzing the different liquid samples.

The frequency response for each sample is then analyzed in terms of the f_s and Q factor by using the CPT for SIW structures [6], [8]

$$\varepsilon_s' = \frac{A\varepsilon_r' V_c}{V_s}\left(\frac{f_0 - f_s}{f_s}\right) + \varepsilon_r' \tag{3a}$$

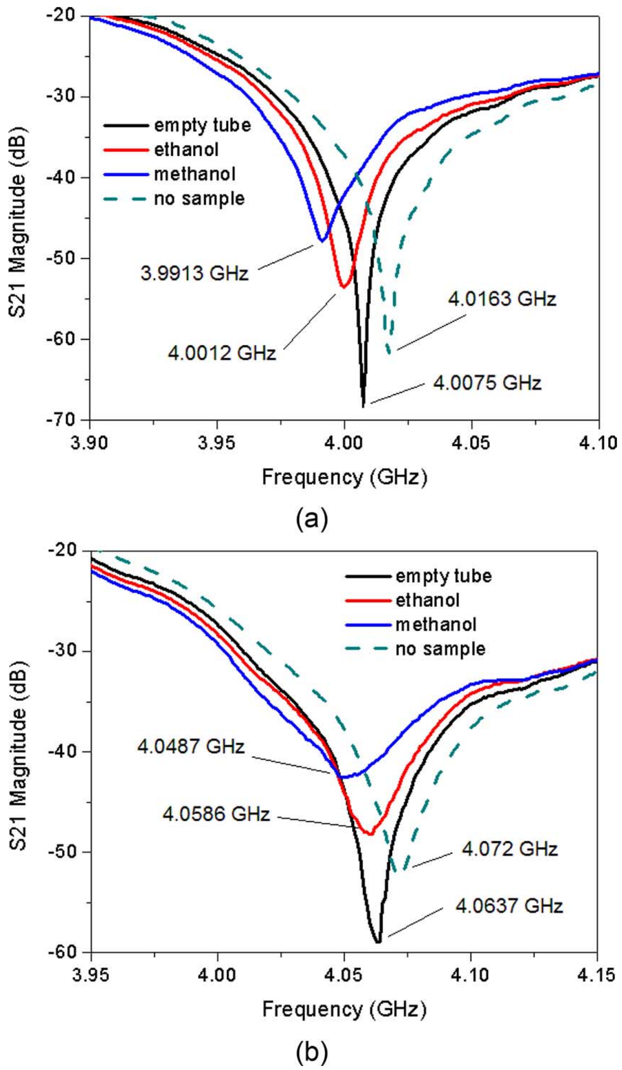

Fig. 12. Measured responses of the system for different samples for $d_s = 1$ cm using: (a) *Tag-A* and (b) *Tag-B*.

$$\varepsilon_s'' = \frac{BV_c}{V_s}\left(\frac{\varepsilon_r'^2 + \varepsilon_r''^2}{\varepsilon_r'}\right)\left(\frac{Q_0 - Q_s}{Q_0 Q_s}\right) + \frac{\varepsilon_s' \varepsilon_r''}{\varepsilon_r'} \tag{3b}$$

with ε' and ε'' being real and imaginary parts of the complex dielectric permittivity; the subscripts r and s indicate the case whether before perturbation or when perturbed with the sample, respectively; f_0 and f_s, as well as Q_0 and Q_s, are the operating frequencies and quality factors before the perturbation and when perturbed with the LUT, respectively; V_c is the volume of the cavity/tunnel and V_s is volume of the sample; A and B are constants related with the configuration of the circuits, mode of operation, shape and position of the sample inside the sensors. As the calculation difficulty of A and B is high, they are obtained experimentally by using standard samples of known dielectric properties [5], [6].

For the analysis, the capillary tube empty (air) is stated as the "before perturbation" case, assuming the dielectric air properties $\varepsilon_r' = 1$ and $\varepsilon_r'' = 0$. The liquids 5) ethanol and 8) methanol are used as the standard samples for calibration of constants A and B, their dielectric values are taken from [21]: $\varepsilon' = 5.47$ and $\varepsilon'' = 4.51$ for ethanol and $\varepsilon' = 15.35$ and $\varepsilon'' = 13.17$ for methanol; both evaluated at 4 GHz and 22 °C.

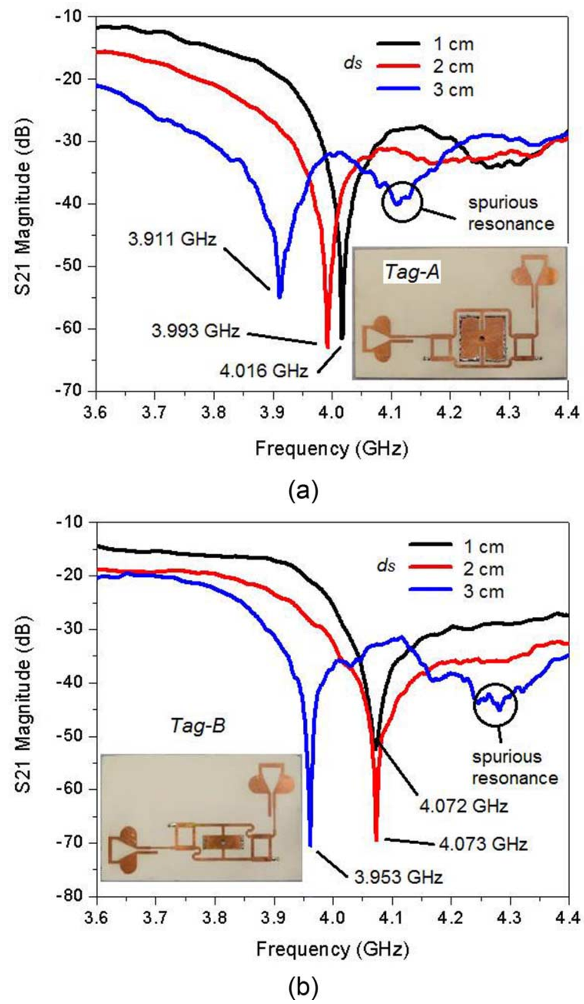

Fig. 13. Measured responses of the system for different d_s values and photographs of: (a) *Tag-A* and (b) *Tag-B*.

TABLE I
CHARACTERIZATION OF LUT USING *TAG-A*:
$V_c = 628.29$ mm^3, $V_s = 1.44$ mm^3

LUT	f_s (GHz)	$d_s = 1$ cm*			f_s (GHz)	$d_s = 2$ cm$^+$		
		Q_s	ε'	ε''		Q_s	ε'	ε''
1	3.9903	54.70	14.67	3.33	3.9634	31.07	15.69	4.04
2	3.9842	53.48	19.54	3.55	3.9594	24.12	18.85	6.52
3	4.0050	46.64	2.98	4.98	3.9802	33.61	2.49	3.39
4	3.9946	34.94	11.24	8.71	3.9740	21.09	7.35	8.10
5	4.0012	44.20	5.99	5.59	3.9755	25.82	6.17	5.79
6	4.0022	37.37	5.20	7.74	3.9770	26.96	4.99	5.35
7	4.0012	36.31	5.99	8.15	3.9755	23.90	6.17	6.62
8	3.9913	32.15	13.87	10.01	3.9663	19.14	13.40	9.39
9	4.0036	41.61	4.09	6.33	3.9775	26.68	4.60	5.46

*$f_0 = 4.0075$ GHz, $Q_0 = 84.20$; $A = 7.25$, $B = 1.19$
$^+f_0 = 3.9821$ GHz, $Q_0 = 58.71$; $A = 7.12$, $B = 0.61$

Tables I and II tabulate the LUT characterization with the system using *Tag-A* and *Tag-B*, respectively, for d_s, 1 and 2 cm.

No LUT characterization is carried out for $d_s = 3$ cm due to the generation of resonances close to the operating frequency and addition of noise levels (Fig. 13), producing difficulties and inaccuracy in obtaining f_s and Q_s values.

TABLE II
CHARACTERIZATION OF LUT USING *TAG-B*: $V_c = 176.19$ mm^3, $V_s = 1.44$ mm^3

LUT	f_s (GHz)	d_s = 1 cm* Q_s	ε'	ε''	f_s (GHz)	d_s = 2 cm$^+$ Q_s	ε'	ε''
1	4.0502	68.65	13.40	4.51	4.0559	24.98	18.08	7.05
2	4.0451	67.64	18.10	5.88	4.0529	23.45	23.55	8.44
3	4.0582	67.08	6.04	6.67	4.0624	26.19	6.26	6.05
4	4.0519	64.62	11.83	10.25	4.0604	22.49	9.89	9.42
5	4.0586	68.33	5.67	4.95	4.0623	27.22	6.44	5.28
6	4.0597	66.55	4.66	7.42	4.0614	25.44	8.08	6.66
7	4.0592	66.00	5.12	8.21	4.0634	21.43	4.45	10.60
8	4.0487	63.56	14.78	11.90	4.0589	21.16	12.62	10.92
9	4.0600	67.55	4.39	6.01	4.0627	28.62	5.72	4.32

*f_0 = 4.0637 GHz, Q_0 = 72.18; A = 30.33, B = 51.62
$^+f_0$ = 4.0653 GHz, Q_0 = 37.19; A = 60.09, B = 4.37

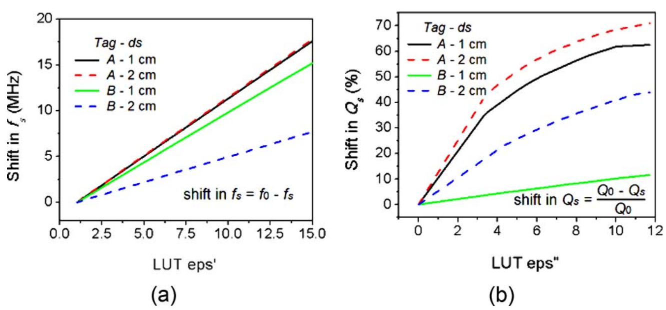

Fig. 14. Sensitivity of the system: (a) ε' of LUT and (b) ε'' of LUT.

TABLE III
SENSITIVITY OF THE TAGS

Tag	***A***		***B***	
ds	*1 cm*	*2 cm*	*1 cm*	*2 cm*
ε'_s (MHz/$\Delta\varepsilon'$)	1.26	1.27	1.09	0.55
ε''_s [ΔQ(%)/$\Delta\varepsilon''$]	6.18	7.18	1.00	3.95

$\Delta\varepsilon'$ and $\Delta\varepsilon''$ are increment in ε'_s and ε''_s of 1;
ΔQ(%) is variation of the measured Q_s in percentage.

VI. DISCUSSIONS OF RESULTS

Fig. 14 shows the sensitivity of the system for f_s and Q_s with both tags (*Tag-A* and *Tag-B*) for ε' and ε'' permittivity parts of the LUT. Shifts in the resonant/tunneling frequencies $(f_0 - f_s)$ and Q factors $[(Q_0 - Q_s)/Q_0(\%)]$ are used for the analysis.

From Fig. 14, it is noticed that a higher sensitivity of the system for ε'_s and ε''_s is obtained using *Tag-A*. Average sensitivities for both tags are shown in Table III.

From Table III, it is noticed that the sensitivity obtained with *Tag-A* is higher than that of *Tag-B* for both ε'_s and ε''_s. For the different distances d_s (1 and 2 cm), *Tag-A* shows almost the same sensitivity for ε'_s; while using *Tag-B*, a sensitivity decrease is observed for a larger distance. For ε''_s, an increase in the sensitivity values are obtained for larger distances d_s using both tags.

Due to the sensitivity variation for different distances between the tag and the reader antennas, position of them must remain constant when analyzing the different samples.

From Tables I and II, it is observed that using *Tag-A*, the averaged differences between the measured and the reported [21] permittivity values of ethanol and methanol (standard samples) are of 9.54% for ε' and 24.03% for ε'' with $d_s = 1$ cm; 12.73% for ε' and 28.49% for ε'' with $d_s = 2$ cm. By using *Tag-B*, the averaged deviations for the same liquids are 3.72% for ε', 9.67% for ε'' with $d_s = 1$ cm; and 17.78%, 17.03% for ε' and ε'', respectively, with $d_s = 2$ cm. This shows that larger the distance between the reader and the tag, the higher the error in the LUT characterization.

The mean ε' and ε'' differences with the samples between the tags operating at 1 and 2 cm antenna separation, respectively, are 25.8% and 24.4% with *Tag-A*; 34.3% and 27.7% using *Tag-B*. Differences and error in the characterization are attributed mainly to influence of noise added to the processed signal.

Observing the maximum energy levels of the processed signals in Fig. 13, estimation of the losses along the whole path are around 20, 25, and 30 dB for both tags at $d_s = 1, 2,$ and 3 cm, respectively. The shift in the resonant/tunneling frequencies for the different distances are attributed to the generation of parasitic resonances close to the operation frequency, as noticed for $d_s = 3$ cm with both tags (Fig. 13).

When no tag is placed, the measured crosstalk levels between the Tx and Rx reader antennas are below -43 dB.

Although the presented system consists of the wireless measurement of liquids at short distances, even inside the near-field region of the planar dipoles, it results ideal for processes requiring continuous monitoring of liquids with a sensing tag fixed at a specific location, such as industrial, medical, and hydrological processes. A possible solution to increase the distance between the reader and tag is to use antennas with higher directivity and gain.

VII. CONCLUSION

A wireless sensing system based on the RFID scheme for the characterization of dielectric permittivity of liquid samples has been presented. The proposed system makes use of the planar technology, considerably reducing the costs of fabrication. Two tags based on different sensors are tested within the system, showing their performance at different distances between the reader and tag. The system shows good sensitivity, low number of elements, and has a high potential for use in real-time testing and monitoring applications. As observed from measurements, the system works well for liquids with dielectric permittivity values lower than 20 evaluated at 4 GHz.

REFERENCES

[1] E. Nyfors, "Industrial microwave sensors—A review," *Subsurf. Sens. Tech. Apps.*, vol. 1, no. 1, pp. 23–43, Jan. 2000.
[2] L. F. Chen, C. K. Ong, C. P. Neo, V. V. Varadan, and V. K. Varadan, *Microwave Electronics, Measurement and Materials Characterization*. New York, NY, USA: Wiley, 2004.
[3] K. Sarabandi and E. S. Li, "Microstrip ring resonator for soil moisture measurements," *IEEE Trans. Geosci. Remote Sens.*, vol. 35, no. 5, pp. 1223–1231, Sep. 1997.
[4] T. Kobayashi and Y. Nikawa, "Dynamic measurement of temperature dependent permittivity of liquid material using microwaves," in *Proc. Asia–Pacific Microw. Conf.*, Yokohama, Japan, Dec. 2010, pp. 1368–1371.
[5] K. Saeed, R. D. Pollard, and I. C. Hunter, "Substrate integrated waveguide cavity resonators for complex permittivity characterization of materials," *IEEE Trans. Microw. Theory Techn.*, vol. 56, no. 10, pp. 2340–2347, Oct. 2008.
[6] H. Lobato-Morales, A. Corona-Chavez, D. V. B. Murthy, and J. L. Olvera-Cervantes, "Complex permittivity measurements using cavity perturbation technique with substrate integrated waveguide cavities," *Rev. Sci. Instrum.*, vol. 81, no. 6, pp. 1–4, Jun. 2010.
[7] A. Alu and N. Engheta, "Dielectric sensing in ε-near-zero narrow waveguide channels," *Phys. Rev. B, Condes. Matter*, vol. 78, no. 4, pp. 1–5, Jul. 2008.

[8] H. Lobato-Morales, D. V. B. Murthy, A. Corona-Chavez, J. L. Olvera-Cervantes, J. Martínez-Brito, and L. G. Guerrero-Ojeda, "Permittivity measurements at microwave frequencies using epsilon-near-zero (ENZ) tunnel structure," *IEEE Trans. Microw. Theory Techn.*, vol. 59, no. 7, pp. 1863–1868, Jul. 2011.

[9] S. Preradovic, I. Balbin, N. C. Karmakar, and G. F. Swiegers, "Multiresonator-based chipless RFID system for low-cost item tracking," *IEEE Trans. Microw. Theory Techn.*, vol. 57, no. 5, pp. 1411–1419, May 2009.

[10] S. Preradovic, N. C. Karmakar, and E. M. Amin, "Chipless RFID tag with integrated resistive and capacitive sensors," in *Proc. Asia–Pacific Microw. Conf.*, Melbourne, Vic., Dec. 2011, pp. 1354–1357.

[11] E. M. Amin and N. C. Karmakar, "Development of a low cost printable humidity sensor for chipless RFID technology," in *Proc. IEEE Int. RFID Tech. App. Conf.*, Nice, France, Nov. 2012, pp. 165–170.

[12] A. Guillet, A. Vena, E. Perret, and S. Tedjini, "Design of a chipless RFID sensor for water level detection," in *Proc. ANTEM*, Tolouse, France, Jun. 2012, pp. 1–4.

[13] D. Girbau, A. Ramos, A. Lazaro, S. Rima, and R. Villarino, "Passive wireless temperature sensor based on time-coded UWB chipless RFID tags," *IEEE Trans. Microw. Theory Techn.*, vol. 60, no. 11, pp. 3623–3632, Nov. 2012.

[14] H. Lobato-Morales, A. Corona-Chavez, and J. L. Olvera-Cervantes, "Planar sensors for RFID wireless complex-dielectric-permittivity sensing of liquids," in *IEEE MTT-S Int. Microw. Symp. Dig.*, Seattle, WA, USA, Jun. 2013.

[15] D. M. Pozar, *Microwave Engineering*, 3rd ed. New York, NY, USA: Wiley, 2005.

[16] EM Circuit Simulator. ver. 13, Sonnet Softw., North Syracuse, NY, USA, 2011.

[17] A. Corona-Chavez, D. V. B. Murthy, and J. L. Olvera-Cervantes, "Novel microwave filters based on epsilon near zero waveguide tunnels," *Microw. Optical Technol. Lett.*, vol. 53, no. 8, pp. 1706–1710, Aug. 2011.

[18] B. Lopez-Garcia, D. V. B. Murthy, and A. Corona-Chavez, "Half-mode microwave filters based on epsilon-near-zero and mu-near-zero concepts," *Prog. Electromagn. Res.*, vol. 113, pp. 379–393, Feb. 2011.

[19] HFSS. ver. 13, Ansoft, Canonsburg, PA, USA, 2010.

[20] X. N. Low, Z. N. Chen, and T. S. P. See, "A UWB dipole antenna with enhanced impedance and gain performance," *IEEE Trans. Antennas Propag.*, vol. 57, no. 10, pp. 2959–2966, Oct. 2009.

[21] A. P. Gregory and R. N. Clarke, "Tables of the complex permittivity of dielectric reference liquids up to 5 GHz," CETM, Teddington, U.K., Nat. Phys. Rep. 33, Jan. 2012.

Humberto Lobato-Morales (S'05–M'14) obtained the B.Sc. and M.Sc. degrees in electronics engineering from the Universidad de las Américas-Puebla (UDLA-P), Puebla, Mexico, in 2006 and 2008, respectively, and the Ph.D. degree in electronics from the Instituto Nacional de Astrofísica, Óptica y Electrónica (INAOE), Puebla, Mexico in 2013.

From 2011 to 2012, he was a Visiting Student with the Electrical Engineering Department, University of California at Los Angeles (UCLA). From 2008 to 2010, he was a Research Engineer with the Emerging Microwaves Technologies EMT Group, INAOE, where he developed microwave techniques for characterization of materials. In October 2013, he joined Centro de Investigación Científica y de Educación Superior de Ensenada (CICESE), Baja California, Mexico, where he is a Researcher with the Electronics and Telecommunications Department. His research interests include microwave filters, multiplexers, antennas, and characterization of materials using microwaves.

Dr. Lobato was the recipient of the IEEE MTT-11 Creativity and Originality in Microwave Measurements Award (2010) and the ROG Most Innovative Design Award (2012).

Alonso Corona-Chávez (SM'09) received the B.Sc. degree in electronics engineering from the Instituto Tecnológico y de Estudios Superiores de Monterrey, Mexico City, Mexico, in 1997, and the Ph.D. degree from the University of Birmingham, Birmingham, Edgbaston, U.K. in 2001. His Ph.D. dissertation concerned microwave beamformers using high-temperature superconductors.

From 2001 to 2004, he was a Microwave Engineer with CryoSystems Ltd. (U.K.), where he developed superconducting front-ends for the telecommunications industry. From 2001 to 2004, he was an Honorary Research Fellow with the Electrical Engineering Department, University of Birmingham, Birmingham, U.K. In September 2004, he joined the Instituto Nacional de Astrofísica, Óptica y Electrónica (INAOE), Puebla, Mexico, where he is currently a Professor with the Electronics Department.

Dr. Corona is a Senior Member of the Institution of Engineering and Technology. He is a Member of the National System for Researchers, Mexico. He was the recipient of a Fulbright Fellowship In April 2009 to carry out research with the Electrical Engineering Department, University of California at Los Angeles (UCLA), Los Angeles, CA, USA.

José Luis Olvera-Cervantes received the B.Sc. degree from the Instituto Politécnico Nacional (IPN), Mexico City, Mexico, in 2001, and the M.Sc. and Ph.D. degrees from the Centro de Investigación Científica y de Educación Superior de Ensenada (CICESE), Baja California, Mexico, in 2005 and 2008, respectively.

As part of his education, he carried out research with the Georgia Institute of Technology, Atlanta, GA, USA, and the Georgia Electronic Design Center (GEDC), Atlanta, GA, USA. In 2009, he joined the Instituto Nacional de Astrofísica, Óptica y Electrónica (INAOE), Puebla, Mexico, where he is a Researcher with the Electronics Department. His research is focused on the characterization of microwave transistors at room and cryogenic temperatures, low-noise amplifiers, microwave filters, and planar antennas.

Dr. Olvera is a Member of the National Institute of Researchers, Mexico.

Ricardo Arturo Chávez-Pérez received the B.Sc. degree in aeronautical engineering from the Instituto Politecnico Nacional (IPN), Mexico City, Mexico, in 1977, the M.Sc. degree in applied physics from the Centro de Investigación Científica y de Educación Superior de Ensenada (CICESE), Baja California, Mexico, in 1990, and the Ph.D. degree in industrial physics engineering from the Universidad Autónoma de Nuevo León (UANL), Nuevo León, México in 2006.

From 1974 to 1980, he was a Research Assistant with the Department of Physics, Centro de Investigación y de Estudios Avanzados (CINVESTAV), Mexico City, Mexico. Since August 1980, he has been with the High-Frequencies Group, CICESE, Baja California, Mexico. His research interests include microwave/millimeter-wave systems design, passive components design, antennas, and development of circuits for breast cancer diagnosis using microwaves.

José Luis Medina-Monroy received the B.Sc. degree from the Universidad de Guadalajara, Guadalajara, Mexico, in 1978, and the M.Sc. and Ph.D. degrees from the Centro de Investigación Científica y de Educación Superior de Ensenada (CICESE), Baja California, Mexico, in 1982 and 1994, respectively.

Since 1982, he has been a Professor and Researcher with the High-Frequencies Group, CICESE. His research interests have been focused on the characterization of microwave transistors, linear and nonlinear analysis, design of low-noise amplifiers, DROs, filters, electromagnetic analysis of planar circuits, on-wafer characterization of pHEMTs and modeling of S-parameters and noise parameters at cryogenic temperatures, design of cryogenic amplifiers, analysis and design of microwave antennas and arrays, as well as the design of RF communication systems up to 40 GHz for satellite and radio-astronomy applications.